Measuring Multiple Potentials of a Rotating and Differentially-Charged Object Simultaneously Using X-rays

Julian Hammerl, Andrea López, Álvaro Romero-Calvo and Hanspeter Schaub

***Abstract*—A method has been proposed to estimate the electric potential of co-orbiting spacecraft remotely using x-rays that are excited by an electron beam. Recent work experimentally investigated the remote electric potential estimation of objects with complex shapes and differentially-charged components, and a new analysis method was proposed that enables the simultaneous measurement of multiple potentials using a single x-ray spectrum. This new analysis method is validated by conducting dynamic experiments where the orientation of the target object changes during the measurement time frame. The particle tracing software SIMION is used to assist the analysis of the experiments. The results show that the new analysis method works for rotating target objects where the electron beam impacts different surfaces over time.**

I. Introduction

Remotely sensing the electric potential of neighboring spacecraft is of interest for spaceflight for several reasons. Knowing the electric potential of each satellite provides a warning for probable electric discharges during docking and servicing operations. Moreover, it improves the performance of charged relative motion control. Electrostatic forces and torques can significantly perturb the relative motion during rendezvous and proximity operations [1]. By feeding forward the estimated electrostatic forces and torques, the control effort for such operations can be reduced [2]. Electrostatic forces can also be utilized to remove retired satellites from geostationary orbit, as proposed for the Electrostatic Tractor [3], [4]. The safety of the Electrostatic Tractor relative motion control is increased with accurate measurements of the electric potential of each spacecraft [5].

Two promising remote electric potential sensing methods have been proposed: The secondary electron method [6] and the x-ray method [7]. Using an electron gun that is attached to a servicing satellite and aimed at the target object, secondary electrons and x-ray are excited from the target and used to estimate the electric potential of the target. Both methods have been validated experimentally [8], [9] for terrestrial conditions in the Electrostatic Charging Laboratory for Interactions between Plasma and Spacecraft (ECLIPS) research vacuum chamber [10].

Recent work on the x-ray method used target objects with complex shapes and differentially-charged components during experiments [11]. A new method was proposed that uses theoretical x-ray models and the principle of superposition of individual x-ray spectra to measure multiple potentials using a single recorded x-ray spectrum. Experiments were conducted in previous work with a large beam landing spot size to excite x-rays from multiple components at a time, demonstrating that this new method can be used for simultaneous measurements. However, the occasion of an electron beam simultaneously hitting multiple components charged to different potentials is rather rare and highly dependent on the geometry of the target object and the electric field. A more realistic scenario is that the electron beam impacts multiple spacecraft components of a rotating object during a given sensing interval. Here a narrow beam is moving across the spacecraft surface and exciting surface elements at different potentials in a sequential rather than parallel manner.

This paper investigates the remote electric potential estimation of a rotating object with complex shapes and differentially-charged components by performing experiments in a vacuum chamber. The goal is to measure multiple potentials simultaneously. An overview of the experimental setup and the particle tracing simulation framework is provided in Sec. II, as well as a fundamental review of the x-ray spectroscopic potential estimation method. The experimental results are shown in Sec. III.

II. Experimental Setup and Theory of Potential Estimation using X-rays

A. Experimental Setup

The experiments are conducted in the ECLIPS Space Environments Simulation Facility [10]. The experimental setup is shown in Fig. 1 and consists of an electron beam, an x-ray detector, and a box-and-panel shaped object on a rotary stage representing a spacecraft bus with one solar panel. The bus of the spacecraft-like target object is a $70 \times 70 \times 70$ mm cube and the panel is a 145×60 mm flat plate. Both components are made of aluminum. Additionally, a Retarding Potential Analyzer (RPA) is included in the setup and used to touchlessly estimate potentials with the electron method [6], but is not required for the x-ray method. The electron beam is a EMG-4212C from Kimball Physics and capable of emitting electrons with energies from 1-30 keV and currents from 1 μA to 100 μA. The focus of the electron beam is adjustable, which allows to either bombard a large area of the target object with electrons, or to focus the electron beam on a small spot.

Julian Hammerl, Andrea López and Álvaro Romero-Calvo are Graduate Research Assistants at the University of Colorado Boulder. E-mail: julian.hammerl@colorado.edu

Hanspeter Schaub is a Professor and Glenn L. Murphy Chair of Engineering at the University of Colorado Boulder

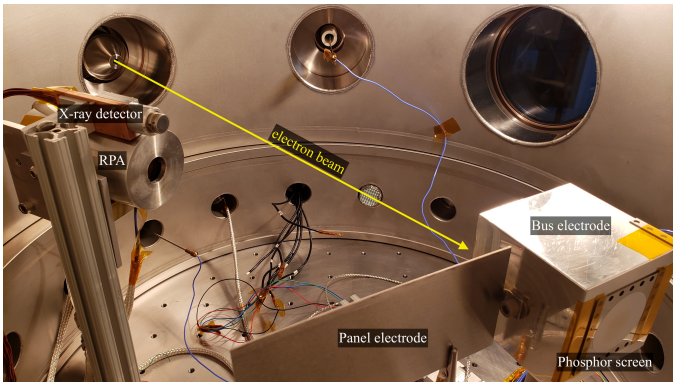

Fig. 1: Experimental setup with a box-and-panel object representing a spacecraft

An Amptek X123 X-ray spectrometer with a 6 mm^2 Si-PIN diode is used to detect the x-rays, and the line between the x-ray detector and the test object approximately forms a $16°$ angle with the electron beam.

A Matsusada AU-30R1 and a Spellman SL300 high voltage power supply separately control the potentials of the spacecraft bus and the panel, and are able two provide potentials up to 30 kV and 1 kV, respectively. The orientation of the spacecraft with respect to the electron beam is varied with a RM-3 vacuum compatible rotary stage from Newmark Systems, and measured with an incremental rotary high-vacuum Renishaw Tonic encoder. The angle is defined to be zero when the panel aligns with the electron beam. A 3.8 cm diameter Kimball Physics Rugged Phosphor Screen is attached to the backside of the test object to verify the landing spot of the unperturbed electron beam (i.e. when both the bus and panel potential are grounded). The unperturbed landing spot of the electron beam is also used as a reference point for the setup of the numerical simulation with the particle tracing software described in the next section.

The orientation for the target object is changed over a time period of 20 seconds, so the electron beam excites x-rays from several components charged to different potentials. The resulting total spectrum is recorded by an x-ray detector over the same time period.

B. Particle Tracing Simulation Framework

A phosphor screen is used to center the electron beam for a specific orientation (-30°) of the uncharged target object, but the exact landing spot of the electron beam on the target object changes with the orientation of the object and the electric potential of the spacecraft bus and panel. However, to validate the experimental results, it is important to know if the electron beam is hitting the bus or panel, because both components are charged to different potentials. Thus, the particle tracing simulation software SIMION[1] is implemented to assist the interpretation of the experimental results. SIMION solves Laplace's equation to derive the electric field and then computes the particle trajectory from Newton's second law. The implementation of the SIMION simulation framework for remote sensing of electric potentials is discussed in greater detail in Ref. [12].

[1]https://simion.com (Consulted on: 03/31/2022)

C. Theory of X-ray Spectroscopic Potential Estimation

Energetic electrons can interact with atoms in various ways. When an inner-shell electron is removed by an incoming energetic electron, an outer-shell electron of the atom fills the vacant spot of the inner-shell, and the difference in energy between the two shells is released as a characteristic x-ray photon [13]. Because the energy difference between shells varies from element to element, the characteristic energy is specific to each element and allows for material identification. Another type of interaction occurs when an electron traverses closely to an atomic nucleus and is decelerated. Again, the loss in energy is emitted as an x-ray photon, called Bremsstrahlung (German for braking radiation) [13]. However, because the interaction with the nucleus can occur in many different paths, the energy of the emitted x-ray is not distinct as for characteristic x-rays, but continuous. The maximum Bremsstrahlung energy is given by the Duane-Hunt law and is equal to the energy of the incident electron prior to the interaction with the atom [14], referred to as the landing energy (or effective energy). Thus, x-ray spectra can be used to estimate the landing energy of the electron beam electrons.

The electron beam interacts with the electric field created by charged objects, and the change in kinetic energy of the electron beam corresponds to the difference in electric potential between the serving satellite (the initial location of the electron beam electrons) and the target object (the final location). Therefore, knowing the electric potential of the servicing satellite, the initial electron beam energy, and estimating the landing energy of the electron beam from x-ray spectra, the potential of the target object can be inferred [7], [9], [15]. For the experiments conducted in the ECLIPS research vacuum chamber, the electron gun is grounded, which corresponds to a neutral potential of the servicing satellite. Consequently, the change in energy of the electron beam is equal to the electric potential of the target object in the vacuum chamber. To estimate the landing energy, it is not sufficient to simply take the energy of the highest energy photon observed by the x-ray detector due to the noise. Instead, a more robust method is recommended by Ref. [16]. Taking advantage of the approximately linear shape of the Bremsstrahlung spectrum close to the landing energy, a linear curve is fitted to the upper energy part of the x-ray spectrum. The energy where this fitted line intersects the x-axis corresponds to the estimated landing energy. This procedure is explained in greater detail in Refs. [9] and [15].

To illustrate the approach for measuring two different potentials simultaneously, theoretical x-ray spectra are created for two different landing energies, representing two different potentials. Reference [17] is used to approximate the characteristic radiation of the theoretical spectrum. The Bremsstrahlung spectrum is approximated using the shape functions from Ref. [18] and the photon energy spectra from Ref. [19], assuming a photon emission angle of $0°$. Figure 2 shows the individual

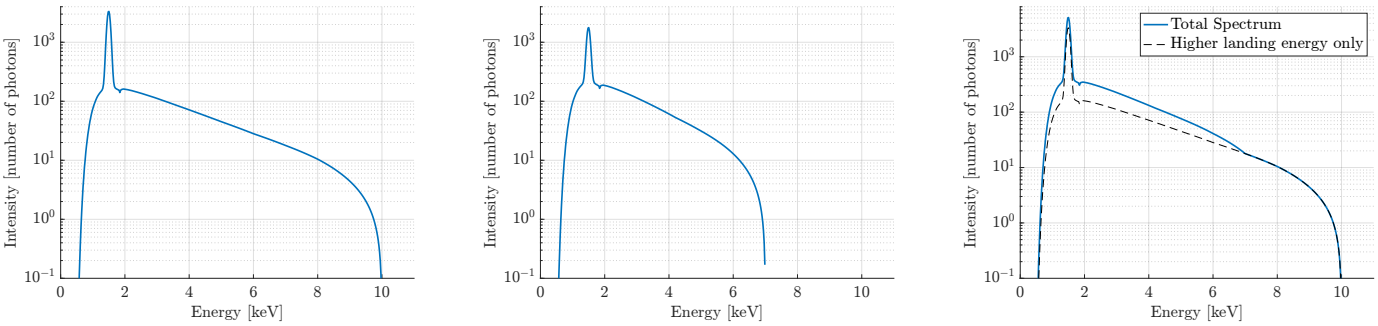

(a) 10 keV Spectrum (b) 7 keV Spectrum (c) Total Spectrum

Fig. 2: Theoretical superposition of X-ray spectra

spectra for a 10 keV and 7 keV landing energy. For an electron beam energy of 10 keV, this corresponds to electric potentials of 0 V and -3 kV, respectively. If an electron beam hits two components charged to different potentials at the same time, then the resulting total spectrum is obtained by superimposing the individual spectra of each landing energy. This is illustrated in Fig. 2c for potentials of 0 V and -3 kV, assuming that the same number of electrons impact both components. A bump is visible in the total spectrum at an energy of 7 keV, which corresponds to the landing energy of the lower-energy individual spectrum. Thus, the lower potential can be estimated by locating this bump in the total spectrum, while the higher potential is estimated from the maximum photon energy of the spectrum.

In a real x-ray spectrum, however, this bump is not easily identified due to the noise in the spectrum. Instead, the higher potential is estimated from the maximum photon energy of the total spectrum, and a theoretical spectrum is computed using the corresponding estimated landing energy. Subtracting the theoretical spectrum from the total spectrum yields a residual spectrum that approximates the individual spectrum of the lower potential component. The lower potential is then estimated by finding the maximum photon energy of the residual spectrum. For example, in Fig. 2, one would estimate the maximum photon energy from the total spectrum (Fig. 2c) and compute the corresponding higher landing energy spectrum (Fig. 2a). The residual spectrum (Fig. 2b) then provides an estimation of the lower landing energy. The two potentials are inferred from the two estimated landing energies. This approach was proposed in Ref. [11].

III. Results

An electron beam spot with a half-cone angle of about $0.5°$ is centered on the phosphor screen for a spacecraft angle of $-30°$ and grounded components. An electron beam current of $I_{EB} = 1$ μA and a beam energy of $E_{EB} = 10$ keV are used. The target object is rotated for $30°$, and a stepper motor speed is chosen such that this takes about 20 seconds. While the object is rotating, an x-ray spectrum is recorded using an accumulation time of 20 seconds, meaning that x-rays of all energies between a few eV and 20 keV are recorded simultaneously during a time frame of 20 seconds. Thus, if the electron impacts different components during the rotation of the target object, the resulting x-ray spectrum includes x-rays excited from both components. Experiments are performed with starting rotation angles between $0°$ and $80°$, in $10°$ steps. Each experiment is repeated 20 times.

Figure 3a shows a sample spectrum for a rotation between $20°$ and $50°$, with a cube potential of -3000 V and a panel potential of -1000 V. The maximum photon energy of about 9 keV is determined using a linear curve fit in the higher energy part of the spectrum as described above. For a beam energy of 10 keV, this corresponds to a potential of -1 kV, i.e. the potential of the spacecraft panel. A theoretical x-ray spectrum is computed for the estimated landing energy of about 9 keV using the models provided by Refs. [17]–[19]. The computed theoretical spectrum agrees well with the measured spectrum (Fig. 3a), and the resulting residual spectrum (the difference between the measured and theoretical spectrum, Fig. 3b) is low in intensity. This suggests that only one potential is detected, and that is the panel potential of -1 kV. This is also confirmed by numerical simulations with SIMION that show that the beam only impacts the spacecraft panel for orientations between $20°$ and $50°$.

The necessary intensity of the theoretical x-ray spectrum to match the recorded spectrum is not exactly known. While it could be computed in theory, such approximation depends on several factors such as the number of electrons impacting the target and the distance between the x-ray source location and the detector. It also assumes that no structures of the target object block the x-ray detector field of view of the source region. These variables are uncertain in a real application, and an accurate intensity of the theoretical spectrum is crucial for the proposed method. Thus, instead of computing the intensity theoretically, the right scaling factor of the intensity is found by fitting the theoretical spectrum to the measured spectrum using least-squares. The fitting region is a 1.5 keV window in the upper end of the spectrum. For example, if the estimated landing energy is 9 keV, then the fitting region is between 7.5 keV and 9 keV. However, this imposes limits on the detection of differential charging. For a fitting window of 1.5 keV, potential differences less than 1.5 kV can not be detected. This also limits how many different potentials can be detected. Only six 1.5 keV windows fit into a spectrum with a maximum energy of 9 keV, restricting the theoretical number of potentials that can be detected to six. The attenuation of low energy x-

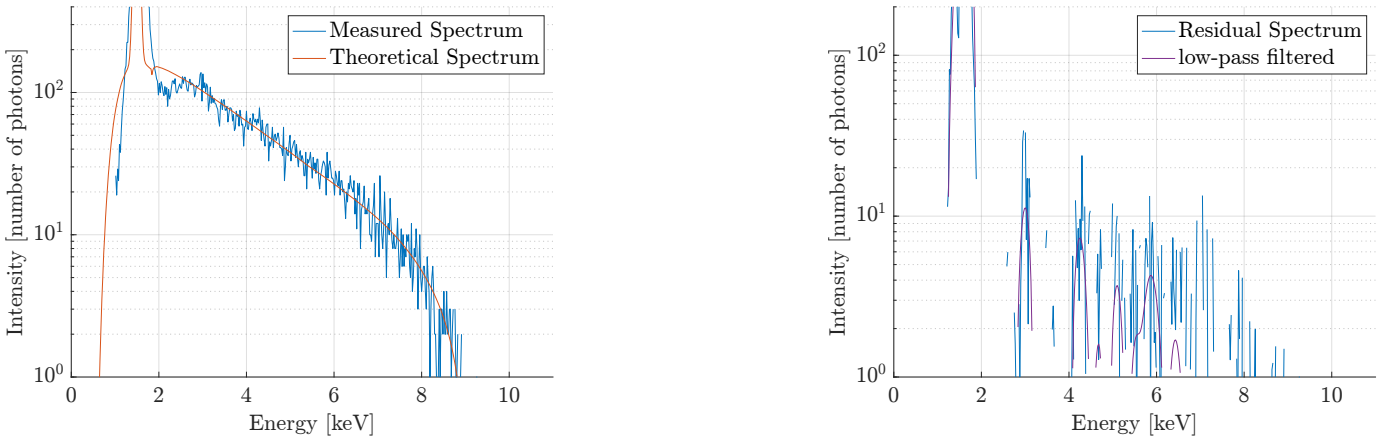

(a) Total Spectrum

(b) Residual Spectrum

Fig. 3: Sample Spectrum for rotation between $20 - 50°$. $\Phi_B = -3000$ V, $\Phi_P = -1000$ V

rays within the x-ray detector likely decreases this number even further.

Another sample spectrum for the same panel and cube potential is shown in Fig. 4a, for a rotation between $80°$ and $110°$. The maximum photon energy is determined and the corresponding theoretical spectrum computed. This time, the measured spectrum clearly deviates from the theoretical one, suggesting that the measured spectrum is a superposition due to multiple different potentials. The residual spectrum in Fig. 4b is high in intensity and consists of what looks like characteristic radiation and bremsstrahlung radiation with a maximum energy of about 7 keV. This suggests that the electron beam impacts another component with a potential of -3 kV in addition to the component with -1 kV.

Experiments are performed for a bus potential of -3 kV and panel potentials of 0 kV and -1 kV. Figure 5 shows the estimated potential for a bus potential of 0 kV and panel potential of -3 kV as a function of the final rotation angle. For example, since rotations of $30°$ are performed, a final rotation angle of $50°$ corresponds to a rotation between $20°$ and $50°$ during which x-rays are measured. Estimation 1 corresponds to the estimation using the total measured spectrum and always measures the highest potential (least negative or most positive potential). Estimation 2 uses the residual spectrum. No second estimation is performed if the residual spectrum is negative between 2 keV and 4 keV, as this is an indicator that likely no second potential is present in the recorded spectrum. In this context, the second potential is the more negative potential. The horizontal bars indicate the 2σ values, where σ is the standard deviation of the 20 runs for a given angle.

As can be seen in Fig. 5, the Estimation 1 accurately measures the potential of the spacecraft panel over all angles. Estimation 2 measures the potential of the cube for higher angles, where the beam impacts the cube. The reason why the second estimation is not as accurate is likely the low intensity of the residual spectrum. In three cases $(30°, 70°, 80°)$, a second estimation is attempted for one of the 20 samples, even though no second potential should be detected for these angles. Figure 6 shows the experimental results for a bus potential of -1 kV and panel potential of -3 kV.

IV. Conclusions

This work investigates the estimation of electric potentials of complex-shaped differentially charged objects using x-ray spectroscopy. The test object is a spacecraft shape primitive with two components that are charged to different potentials. By looking at the maximum energy of the recorded x-rays, only the higher potential – either more positive or less negative – can be estimated. A new approach was proposed in prior work that uses theoretical x-ray models to estimate multiple potentials of differentially charged objects with a single recorded x-ray spectrum.

Dynamic experiments are performed with a target object that is rotating while the x-ray detector is counting x-rays. The experimental results show that it is possible to estimate multiple potentials simultaneously of a rotating, differentially charged target object using the proposed method. Moreover, the results suggest that the presence of a second potential in the recorded x-ray spectrum does not interfere with the estimation of the higher potential. The results of the conducted experiments with a rotating target object are promising as uncooperative target objects in orbit may tumble at high rates.

Acknowledgments

The authors would like to thank Dr. Kieran Wilson for fruitful discussions. This work was supported by U.S. Air Force Office of Scientific Research under grant FA9550-20-1-0025. A.R.C. thanks the *la Caixa* Foundation (ID 100010434, agreement LCF/BQ/AA18/11680099) and the Rafael del Pino Foundation for their financial support.

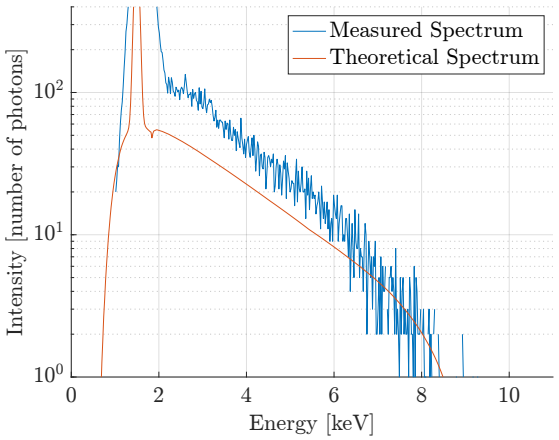

(a) Total Spectrum

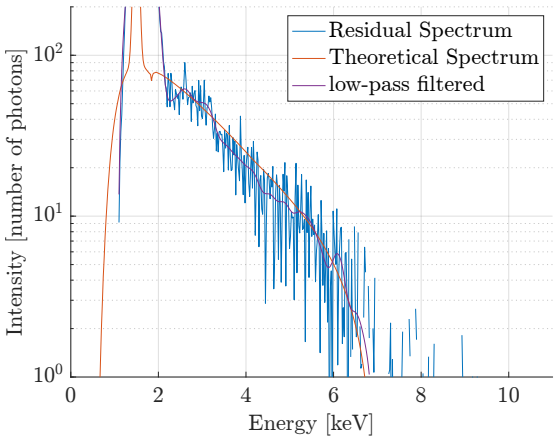

(b) Residual Spectrum

Fig. 4: Sample Spectrum for rotation between $80 - 110°$. $\Phi_B = -3000$ V, $\Phi_P = -1000$ V

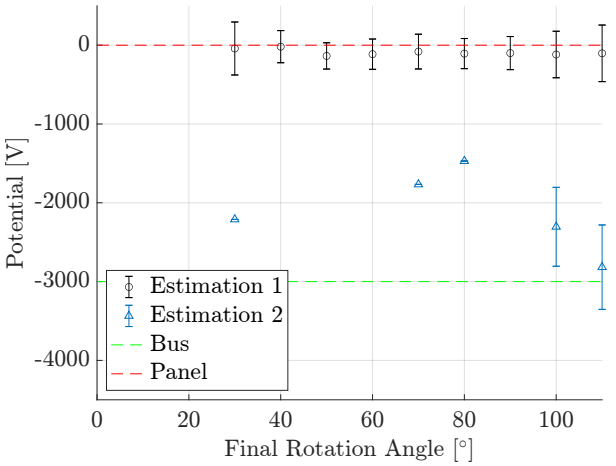

Fig. 5: Dynamic Experiment Results. $\Phi_B = -3000$ V, $\Phi_P = 0$ V

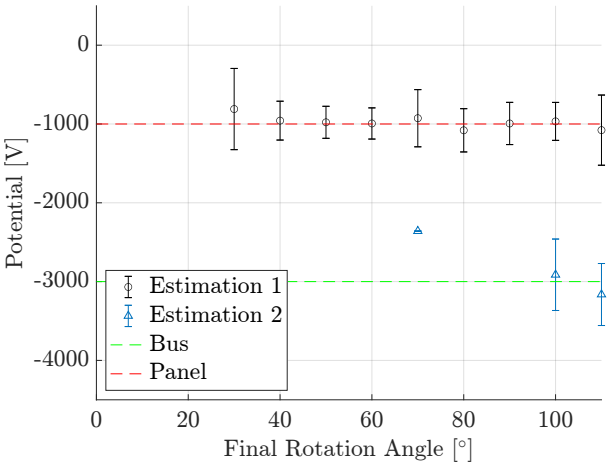

Fig. 6: Dynamic Experiment Results. $\Phi_B = -3000$ V, $\Phi_P = -1000$ V

REFERENCES

[1] K. Wilson and H. Schaub, "Impact of Electrostatic Perturbations on Proximity Operations in High Earth Orbits," *Journal of Spacecraft and Rockets*, vol. 58, no. 5, pp. 1293–1302, 2021.

[2] K. Wilson, Á. Romero-Calvo, and H. Schaub, "Constrained Guidance for Spacecraft Proximity Operations Under Electrostatic Perturbations," *Journal of Spacecraft and Rockets*, pp. 1–13, Mar. 2022, in press.

[3] H. Schaub and D. F. Moorer, "Geosynchronous Large Debris Reorbiter: Challenges and Prospects," *The Journal of the Astronautical Sciences*, vol. 59, no. 1-2, pp. 161–176, Jun. 2012.

[4] M. Bengtson, K. Wilson, J. Hughes, and H. Schaub, "Survey of the electrostatic tractor research for reorbiting passive GEO space objects," *Astrodynamics*, vol. 2, no. 4, pp. 291–305, Dec. 2018.

[5] J. Hammerl and H. Schaub, "Effects of Electric Potential Uncertainty on Electrostatic Tractor Relative Motion Control Equilibria," *Journal of Spacecraft and Rockets*, vol. 59, no. 2, pp. 552–562, Mar. 2022.

[6] M. Bengtson, J. Hughes, and H. Schaub, "Prospects and Challenges for Touchless Sensing of Spacecraft Electrostatic Potential Using Electrons," *IEEE Transactions on Plasma Science*, vol. 47, no. 8, pp. 3673–3681, Aug. 2019.

[7] K. Wilson and H. Schaub, "X-Ray Spectroscopy for Electrostatic Potential and Material Determination of Space Objects," *IEEE Transactions on Plasma Science*, vol. 47, no. 8, pp. 3858–3866, Aug. 2019.

[8] M. T. Bengtson, K. T. Wilson, and H. Schaub, "Experimental Results of Electron Method for Remote Spacecraft Charge Sensing," *Space Weather*, vol. 18, no. 3, Mar. 2020.

[9] K. T. Wilson, M. T. Bengtson, and H. Schaub, "X-ray Spectroscopic Determination of Electrostatic Potential and Material Composition for Spacecraft: Experimental Results," *Space Weather*, vol. 18, no. 4, pp. 1–10, Apr. 2020.

[10] K. Wilson, Á. Romero-Calvo, M. Bengtson, J. Hammerl, J. Maxwell, and H. Schaub, "Development and characterization of the ECLIPS space environments simulation facility," *Acta Astronautica*, vol. 194, no. July 2021, pp. 48–58, May 2022.

[11] J. Hammerl, Á. Romero-Calvo, A. López, and H. Schaub, "Touchless Potential Sensing of Complex Differentially-Charged Shapes Using X-Rays," in *AIAA Scitech 2022 Forum*, San Diego, CA, Jan. 2022, pp. 1–13.

[12] Á. Romero-Calvo, J. Hammerl, and H. Schaub, "Touchless Potential Sensing of Differentially-Charged Spacecraft Using Secondary Electrons," *Journal of Spacecraft and Rockets*, 2022, accepted.

[13] L. Reimer, *Scanning Electron Microscopy*, ser. Springer Series in Optical Sciences. Berlin, Heidelberg: Springer Berlin Heidelberg, 1998, vol. 45.

[14] W. Duane and F. L. Hunt, "On X-Ray Wave-Lengths," *Phys. Rev.*, vol. 6, no. 2, pp. 166–172, Aug. 1915.

[15] K. T. H. Wilson, "Remote Electrostatic Potential Determination for Spacecraft Relative Motion Control," Doctoral Thesis, University of Colorado Boulder, 2021.

[16] M. Lamoureux and P. Charles, "General deconvolution of thin-target and thick-target Bremsstrahlung spectra to determine electron energy distributions," *Radiation Physics and Chemistry*, vol. 75, no. 10, pp. 1220–1231, 2006.

[17] G. H. McCall, "Calculation of X-ray bremsstrahlung and characteristic

line emission produced by a Maxwellian electron distribution," *Journal of Physics D: Applied Physics*, vol. 15, no. 5, pp. 823–831, May 1982.

[18] L. Kissel, C. Quarles, and R. Pratt, "Shape functions for atomic-field bremsstrahlung from electrons of kinetic energy 1–500 keV on selected neutral atoms $1 \leq Z \leq 92$," *Atomic Data and Nuclear Data Tables*, vol. 28, no. 3, pp. 381–460, May 1983.

[19] R. H. Pratt, H. K. Tseng, C. M. Lee, L. Kissel, C. MacCallum, and M. Riley, "Bremsstrahlung energy spectra from electrons of kinetic energy 1 keV $\leq$ T1 $\leq$ 2000 keV incident on neutral atoms $2 \leq Z \leq 92$," *Atomic Data and Nuclear Data Tables*, vol. 20, no. 2, pp. 175–209, 1977.